Reduced Evapotranspiration Decreases Land Precipitation despite Enhanced Moisture Convergence: Insights from Perturbed Parameter Ensembles of Earth System Models

BENJAMIN G. BUCHOVECKY,[a] F. HUGO LAMBERT,[b] CLAIRE M. ZARAKAS,[a] MARYSA M. LAGUË,[c] CHARLES D. KOVEN,[d] INEZ Y. FUNG,[e] DAVID B. BONAN,[a,f] AND ABIGAIL L. S. SWANN[a,g]

[a] *Department of Atmospheric and Climate Science, University of Washington, Seattle, Washington*
[b] *Department of Mathematics and Statistics, University of Exeter, Exeter, United Kingdom*
[c] *Department of Geography, The University of British Columbia, Vancouver, British Columbia, Canada*
[d] *Climate and Ecosystem Sciences Division, Lawrence Berkeley National Laboratory, Berkeley, California*
[e] *Department of Earth and Planetary Science, University of California, Berkeley, Berkeley, California*
[f] *Cooperative Institute for Climate, Ocean, and Ecosystem Studies, University of Washington, Seattle, Washington*
[g] *Department of Biology, University of Washington, Seattle, Washington*

(Manuscript received 22 December 2025, in final form 24 September 2026, accepted 15 October 2026)

ABSTRACT: Both canonical theory and climate model simulations predict an increase in globally averaged precipitation with radiatively forced warming. However, terrestrial processes control surface water and energy fluxes and, therefore, can impact surface temperatures independently of radiative forcing. Here, we investigate the sensitivity of the global hydrological cycle to warming induced by changes in land surface conditions using perturbed parameter ensembles from two climate models, which sample a broad range of evapotranspiration (ET) states through modifications to land model parameters. The parameters are perturbed within the range of observationally constrained uncertainty and alter ET through different land surface pathways. We find that reduced ET drives warming yet decreases land-mean precipitation, which we link to strong decreases in near-surface relative humidity from warming. These decreases in relative humidity overcome increases in specific humidity and moisture convergence over land, which are also caused by shifts in large-scale circulation. We explain the tropical precipitation response to ET forcing with a simple scaling that relates changes in the land–ocean contrast in relative humidity to land-mean precipitation change. Further, the suppressed ET induces a shortwave cloud response that amplifies warming. Our results highlight that changes to land surface properties at the magnitude of parametric uncertainty influence warming and precipitation. ET-driven warming reduces land precipitation, opposite in sign to the precipitation increase from radiatively forced warming. This response is not directly captured by scalings of the global hydrological cycle with radiative forcing. We, therefore, establish the potential significance of terrestrial ecosystem functioning, and its response to climate change, for hydroclimate.

SIGNIFICANCE STATEMENT: Increasing the concentration of atmospheric greenhouse gases leads to global warming and drives changes in precipitation, with precipitation increasing when averaged globally. While greenhouse gases are the dominant driver of climate change, other processes can also influence temperature and precipitation to a secondary degree. In particular, land processes can directly influence surface temperatures by controlling the transfer of water and energy from the land to the atmosphere. In this study, we analyze ensembles of global climate model simulations with modified land parameters. In these simulations, warming is due to changes in land physical properties rather than changes in greenhouse gas concentrations. We find that when warming is driven by reduced land evapotranspiration (ET), this warming is associated with precipitation decreases over land. This occurs because reducing ET decreases relative humidity and changes clouds. Our results highlight how the relationship between precipitation and temperature differs when comparing the impact of land ET versus greenhouse gases. We expect that changes to ecosystems and land physical properties under climate change will alter ET, and our results indicate the importance of these land surface changes to global precipitation.

KEYWORDS: Atmosphere-land interaction; Precipitation; Evapotranspiration; Moisture/moisture budget; Climate models

1. Introduction

Over land, evapotranspiration (ET) returns over half of precipitation back to the atmosphere, making it the dominant pathway connecting the terrestrial hydrological cycle to the broader atmospheric hydrological cycle (Trenberth et al. 2007). By converting net incoming radiation into latent heat instead of sensible heat, ET simultaneously regulates near-surface air temperature and atmospheric moisture supply, shaping the thermodynamic conditions that govern boundary layer growth and convection (e.g., Eltahir 1998; Langenbrunner et al. 2019; van der Drift and O'Gorman 2025) and large-scale circulation (e.g., Kooperman et al. 2018; Laguë et al. 2023). In idealized climate model simulations, strongly suppressing terrestrial ET induces a global hydrological response characterized by a decrease in precipitation and a positive shortwave cloud feedback alongside significant near-surface warming (Laguë et al. 2023). Notably,

Supplemental information related to this paper is available at the Journals Online website: https://doi.org/10.1175/JCLI-D-25-0739.s1.

Corresponding author: B. G. Buchovecky, bbucho@uw.edu

DOI: 10.1175/JCLI-D-25-0739.1

© 2026 American Meteorological Society. This published article is licensed under the terms of the default AMS reuse license. For information regarding reuse of this content and general copyright information, consult the AMS Copyright Policy (www.ametsoc.org/PUBSReuseLicenses).

Brought to you by University of Washington Libraries | Unauthenticated | Downloaded 11/20/26 03:51 PM UTC

declining precipitation with warming is opposite in sign to the precipitation response under radiatively forced warming (Allen and Ingram 2002; Held and Soden 2006; O'Gorman et al. 2012). The sensitivity of global precipitation to large ET perturbations demonstrated by these idealized experiments raises a critical question: Do realistic perturbations to ET from land surface processes drive global precipitation responses? Here, we evaluate the sensitivity of the global hydrological cycle to generalized ET forcing agnostic to any specific land process pathway by sampling observationally constrained terrestrial parametric uncertainty using perturbed parameter ensembles across two climate models. We contrast the resulting hydrological response with that of radiatively forced warming.

While climatological ET is set by a competition between the atmospheric demand for water vapor and the supply of water from precipitation (Budyko 1974), ET is not a fixed property of the land surface. The land surface influences ET variability through two core pathways: soil water availability, which determines the water supply to the land surface, and plant processes, which regulate the biological conductance of water vapor to the atmosphere through transpiration and canopy growth. Prior work has characterized how each of these controls independently drives ET anomalies and associated precipitation responses. However, these process-specific studies focus on experiments that apply large changes to land surface functioning without sampling the full range of uncertainty, motivating a more generalized treatment of ET as a land surface forcing.

Soil moisture integrates precipitation inputs, ET losses, and runoff, making it the primary state variable governing the terrestrial water supply for ET. As such, understanding how soil moisture influences ET and precipitation has been a long-standing research focus (e.g., Shukla and Mintz 1982). Whether soil moisture anomalies propagate into ET anomalies depends on the local coupling regime: ET is sensitive to soil moisture in water-limited regions, while ET is constrained by net radiation and largely insensitive to soil moisture in energy-limited regions (Budyko 1974). However, the strength of the coupling between soil moisture and ET varies across climate models depending on the pattern of mean precipitation simulated by each model (Berg and Sheffield 2018). The effect of soil moisture typically is quantified by comparing climate model simulations where soil moisture is prescribed or allowed to freely evolve, as in the Global Land–Atmosphere Coupling Experiment (GLACE; Koster et al. 2006, 2010; Seneviratne et al. 2013). All other initial conditions and boundary conditions remain constant between the two experiments, including sea surface temperatures (SSTs) which may dampen the large-scale circulation response (Chou et al. 2009; Bony et al. 2013). Both GLACE-1 (Koster et al. 2006) and GLACE-2 (Koster et al. 2010) experiments prescribe daily climatological soil moisture to isolate the influence of seasonal to subseasonal soil moisture variability on precipitation. These experiments show that variability in soil moisture explains a meaningful fraction of the variance in precipitation, with multiple semiarid "hotspot" regions exhibiting much stronger soil moisture–precipitation coupling (Koster et al. 2006; Guo et al. 2006; Koster et al. 2010). Notably, the strength of the ET–precipitation relationship has larger intermodel spread than the soil moisture–ET relationship (Guo et al. 2006).

As a by-product of their design, these subseasonal soil moisture variability experiments also perturb mean state ET. Prescribing climatological soil moisture tends to lead to higher ET in regions where soil moisture oscillates between near saturated after rainfall and much lower saturated between rainfall events (Krakauer et al. 2010). In a set of simulations similar to GLACE, Krakauer et al. (2010) find that mean ET over land decreased by 8% in the interactive soil moisture simulation compared to the climatological soil moisture simulation, corresponding to a 5% decrease in land precipitation. Moisture convergence over land remained near constant between the two experiments, implying that reductions in ET primarily change precipitation recycling over land and not water vapor transport.

Similar results emerge from the GLACE Coupled Model Intercomparison Project phase 5 (CMIP5) experiments which isolated the influence of long-term soil moisture trends on climate under the high-emission RCP8.5 scenario (Seneviratne et al. 2013). Berg et al. (2016) show that reductions in soil moisture decrease ET, relative humidity, and precipitation over land which increases aridity relative to simulations without reductions in soil moisture. Using the same GLACE-CMIP5 simulations, Zhou et al. (2021) demonstrate that soil moisture exerts a strong control on precipitation minus evaporation ($P - E$) over dry lands. Soil moisture reductions suppress ET, which in turn reduces precipitation, with ET declining at roughly twice the rate of precipitation. At the same time, the decline in ET warms the land surface and drives vertical ascent which enhances moisture convergence and $P - E$. The net effect is a strong negative soil moisture feedback on $P - E$ over dry lands. Interestingly, these results contrast with the near invariance of moisture convergence over the global land mean in Krakauer et al. (2010), suggesting that moisture convergence in regions outside of dry lands decreases to compensate. In a more recent study, Zhou et al. (2023) further corroborate the relationship between soil moisture, ET, and precipitation using simulations with and without interactive soil moisture, finding that reductions in soil moisture suppress both ET and precipitation over land, and these soil moisture–induced changes are necessary to capture drying trends in response to anthropogenic warming.

Other aspects of the land surface besides soil moisture also can control ET. Stomatal conductance and leaf area both respond to elevated atmospheric carbon dioxide (CO_2) concentrations, modulating transpiration and canopy evaporation independently of soil moisture, which combined together we call the physiological effect. Reductions in stomatal conductance tend to dominate the physiological effect in many, but not all, Earth system model experiments, driving decreases in ET and precipitation over land (Betts et al. 1997, 2007; Swann et al. 2016; Berg et al. 2016; Skinner et al. 2017; Chadwick et al. 2019; Zhang et al. 2024). The ET response, however, is more variable across models from CMIP6 (e.g., Zarakas et al. 2020; Mankin et al. 2025). Isolating the temperature influence from the total physiological effect, Chadwick et al. (2019) find that the physiological effect decreases precipitation due to lower moisture supply while the warming from reduced transpiration alone increases moisture convergence and precipitation. These results support prior work that stomatal closure without changes to leaf

Brought to you by University of Washington Libraries | Unauthenticated | Downloaded 11/20/26 03:51 PM UTC

area increases precipitation over land due to warming and associated enhanced moisture convergence (Betts et al. 2007; Pu and Dickinson 2014). However, the physiological effect has strong spatial patterns, as illustrated by Kooperman et al. (2018) which finds that the physiological effect drives a zonal precipitation asymmetry characterized by increases in precipitation over Asian and African tropical forests and decreases over South American forests. Pietschnig et al. (2019) confirm these results using experiments with idealized continental configurations and find that precipitation change is strongly linked to changes in near-surface relative humidity. A similar set of idealized experiments shows that the spatial continental extent ultimately determines whether the physiological effect increases or decreases precipitation due to the competition between increased moisture convergence and reduced ET (Pietschnig et al. 2021).

These soil moisture and physiological effect studies demonstrate that land surface processes can substantially influence precipitation through ET, making ET an important part of hydroclimate projections. Yet, ET remains one of the most uncertain components of the terrestrial water cycle because it arises from nonlinear interactions between biological, ecological, and physical climate processes that are difficult to constrain with observations. Uncertainty in land process representation has been shown to meaningfully impact ET and drive temperature changes (Zarakas et al. 2024b). Additional uncertainty arises because the atmospheric response to ET can dampen the initial ET change in wet regions via a reduction in vapor pressure deficit which suppresses evaporative demand (Zarakas et al. 2024a). Crucially, the biological and ecological adjustments that govern these land-driven climate responses are largely independent of the radiatively forced climate signal.

In contrast to the land surface ET-driven uncertainty, the globally averaged precipitation response to radiative forcing and its associated warming is relatively well characterized. While saturation vapor pressure of water scales with temperature at ~7% K^{-1} following the Clausius–Clapeyron equation, global-mean precipitation increases at only ~2%–3% K^{-1} (Allen and Ingram 2002; Held and Soden 2006; Fläschner et al. 2016; Pendergrass 2020; Allan et al. 2020). On long time scales, the increase in precipitation with warming is constrained by Earth's energy balance: Latent heat released through precipitation must be balanced by radiative cooling from longwave and shortwave radiation in the atmosphere and sensible heat at the surface. The efficiency of atmospheric radiative cooling thus provides a limit on the increase in global-mean precipitation (Lambert and Webb 2008; Stephens and Ellis 2008; O'Gorman et al. 2012; Pendergrass and Hartmann 2014; DeAngelis et al. 2015). Over land, precipitation tends to increase at a lower rate of ~0.8%–2.4% K^{-1} due to amplified warming and aridity over land (Samset et al. 2018; Richardson et al. 2018; Allan et al. 2020). These precipitation changes will in turn affect ET in moisture-limited regions which may feed back on precipitation.

Prior process-specific experiments establish that large ET perturbations drive precipitation change, but by design, they do not assess the response to generalized ET forcing irrespective of the forcing pathway or whether ET uncertainty stemming from realistic land surface parameter uncertainty produces a comparable response. In this study, we quantify the precipitation response to ET perturbations within the range of observationally constrained terrestrial parametric uncertainty relative to the precipitation response to CO_2. This comparison situates the land surface–driven precipitation response in the same quantitative framework as the canonical atmospheric response to forcing. We analyze two ensembles of climate model simulations forced by either ET or atmospheric CO_2, allowing us to isolate the precipitation response to nonradiative ET forcing from that to radiative forcing. Unlike prior work centered on soil moisture feedbacks or the plant physiological effects, we do not prescribe a specific land surface process as the driver. Instead, we exploit terrestrial parametric uncertainty to generate a wide but plausible range of ET perturbations emerging from diverse biological and physical land surface pathways, treating them as a generalized forcing and examining the resulting atmospheric response. We further allow SSTs to change in response to ET forcing to better capture large-scale shifts in circulation, differing from the GLACE experiments which are not able to capture that effect (e.g., Berg et al. 2016; Zhou et al. 2021).

Across two climate models and three ensembles of simulations, we find that reduced ET and its associated warming increase moisture convergence over land but reduce land precipitation, which we link to significant decreases in relative humidity. Reductions in ET also induce a shortwave cloud feedback that amplifies land warming. Section 2 describes the model simulations used and methods for analyzing moisture convergence and precipitation change. Section 3 contains our results and discussion of ET-driven warming, shortwave cloud feedbacks, and global hydrological responses over land. We present our summary and conclusions in section 4.

2. Model simulations

a. *Perturbed parameter ensembles*

We examine land nonradiative forcings to the global hydrological cycle using two perturbed parameter ensembles (PPEs): one from the Community Earth System Model, version 2 (CESM2; Danabasoglu et al. 2020), and one from the Hadley Centre Coupled Model, version 3 (HadCM3C; Booth et al. 2012). The CESM2 preindustrial (PI) PPE, described further in Zarakas et al. (2024b), was run in a coupled atmosphere–land–slab ocean configuration using the Community Land Model, version 5 (CLM5; Lawrence et al. 2019), with prognostic leaf area; the Community Atmosphere Model, version 6 (CAM6; Bogenschutz et al. 2018), with fixed PI greenhouse gas concentrations; and a slab ocean model (SOM; Danabasoglu and Gent 2009) which represents the ocean as a single thermodynamic mixed layer. The CESM2 PI PPE simulations have a horizontal grid resolution of 1.9° latitude × 2.5° longitude with 32 vertical layers in the atmosphere. The CESM2 PI PPE (Zarakas et al. 2024b) sampled 18 parameters in CLM5 across different functional areas of the model, including soil hydrology, stomatal conductance, photosynthesis, and canopy evaporation (Table S1 in the online supplemental material). The selected parameters were then set one at a time to a minimum and maximum value informed by literature review and expert judgment (Kennedy et al. 2025) for a total of 36 simulations plus one control simulation with the default

Brought to you by University of Washington Libraries | Unauthenticated | Downloaded 11/20/26 03:51 PM UTC

TABLE 1. Summary of simulations used in this study. The CO_2 concentrations for the HadCM3C PPE are computed as the average over the 50-yr analysis period and display the range across the ensemble due to parameter-induced differences in carbon cycle feedbacks.

Name	Experiment type	CO_2 concentration		Total simulations
		Control (ppm)	Experiments	
CESM2 PI PPE	Perturbed land parameters	284	284 ppm	36
HadCM3C Hist PPE	Perturbed land parameters	331	321–343 ppm	16
HadCM3C A1B PPE	Perturbed land parameters	753	590–927 ppm	16
CMIP6 CO_2	Abrupt change in CO_2 from the preindustrial concentration	284	142 ppm 0.5 × CO_2 568 ppm 2 × CO_2 1136 ppm 4 × CO_2	21

CLM5 parameter set (Table 1). Important for our analysis here, the parameter perturbations induced surface temperature change and precipitation change largely by modifying ET rather than land albedo or aerodynamic surface roughness (Figs. S1a–c). Zarakas et al. (2024b) found that the evaporative fraction, defined as the ratio of latent heat flux (i.e., ET in energy units) to the sum of latent and sensible heat fluxes, accounted for half of the variance in global-mean temperature change across the CESM2 PI PPE, while albedo accounted for less than 10% of the variance. Thus, the CESM2 PI PPE uniquely provides a set of simulations at constant preindustrial CO_2 levels where land ET primarily drives surface climate change instead of radiative forcing. To isolate the climate response to parameter perturbations, we subtract the control simulation that used default parameters from each perturbed parameter ensemble member.

In addition to the CESM2 PI PPE, we analyze two scenarios of a PPE (Booth et al. 2012) from the HadCM3C model: one forced with historical greenhouse gas emissions and aerosol concentrations from 1850 to 1990 and the other forced with projected greenhouse gas emissions from 1990 to 2100 A1B SRES scenario (Nakicenovic et al. 2000). Hereafter, we refer to the historical scenario as "Hist" and the future scenario as "A1B." HadCM3C was run in a configuration using a flux-adjusted version of HadCM3 (Gordon et al. 2000) with fully dynamic atmosphere and ocean components coupled to a land surface model with dynamic vegetation (TRIFFID; Cox 2001; Cox et al. 2000). Unlike CLM5, TRIFFID allows plant types within the model to alter their spatial distribution based on environmental conditions and competition with other plant types. HadCM3C PPE has a horizontal grid resolution of 2.5° latitude × 3.75° longitude for the atmosphere and land, with a higher resolution of 1.25° latitude × 1.25° longitude ocean model. Adjustments to ocean surface heat and water fluxes were calibrated relative to an observed climatology during an initial integration and then iteratively applied in subsequent simulations to correct errors in ocean transport and ocean–atmosphere exchanges (Falloon et al. 2012). The configuration also included a complete coupled carbon cycle with prognostic CO_2, such that climate–carbon cycle feedbacks to the emission forcings prognostically set the atmospheric CO_2 concentration (Booth et al. 2012; Lambert et al. 2013). The HadCM3C PPE used the same parameter perturbations for each scenario, sampling six land surface and terrestrial carbon cycle parameters with a Latin hypercube approach for a total of 16 simulations in each ensemble plus one control simulation that used the default parameter set (Table 1 and Table S2). For the HadCM3C Hist and A1B PPE simulations, forcing and climate are transiently changing through each run. Since the transient forcing is identical in all ensemble members, we remove the mean effect of the transient climate and calculate the effect of a parameter perturbation by subtracting the control member that used default parameters from each perturbed parameter ensemble member. Other feedback effects, including on atmospheric CO_2 (described below), will still alter the transient trajectory of climate, and these will be captured as a response of climate to each parameter perturbation.

Unlike the CESM2 PI PPE in which temperature changes over land were largely driven by changes in ET, the parameter perturbations in the two scenarios of the HadCM3C PPE generated significant spread in both surface albedo and ET over land (Fig. S1), making it difficult to cleanly disentangle a primary driver of surface temperature change. Dynamic vegetation in HadCM3C generated a greater spread in surface albedo in the northern high latitudes, resulting from the different albedos of plant functional types and the changing spatial distribution of plant functional types due to competition and evolving environmental conditions (Figs. S2 and S3). Furthermore, the parameter perturbations induced carbon cycle feedbacks in HadCM3C which generated a spread in atmospheric CO_2 concentrations and thus radiative forcing, even after subtracting out the default parameter simulation. The spread in CO_2 across the ensemble members grew to 466 ppm by the end of the century which approximately corresponds to a spread of 2.83 W m^{-2} of radiative forcing at the top of the atmosphere (Fig. S4). Over the 50-yr analysis period from 2050 to 2100 in the A1B PPE, the range across the ensemble in the time-mean CO_2 concentration is 337 ppm. Despite these additional feedbacks which create more axes of variation compared to the CESM2 PI PPE, we nonetheless include these simulations because to our knowledge they are the only other set of experiments where land model parameters are perturbed across a range of values in a fully coupled climate model.

b. *CMIP6 CO_2 simulations*

The PPE simulations have variations in climate that are driven directly by changes in land surface functioning. We compare

Brought to you by University of Washington Libraries | Unauthenticated | Downloaded 11/20/26 03:51 PM UTC

these nonradiative land forcings with radiative forcing from CO_2 by comparing the CESM2 PI PPE and HadCM3C PPE to idealized simulations using fully coupled climate models participating in CMIP6 (Eyring et al. 2016). Specifically, we use experiments where atmospheric CO_2 is abruptly halved, doubled, or quadrupled relative to preindustrial concentrations and refer to the collection of these experiments as the CO_2 ensemble. These CMIP6 models have fully dynamic atmosphere and ocean components with prescribed CO_2 levels. For our analysis, we selected the seven models with available monthly output for each abrupt CO_2 change experiment for a total of 21 simulations (Table 1 and Table S3). To quantify the response to CO_2 radiative forcing for each model, we subtract the simulation with preindustrial CO_2 levels from the simulations with altered CO_2 levels. Grouping these CMIP6 experiments together allows us to quantify the hydrological response to radiatively forced warming across a range of atmospheric CO_2 concentrations.

c. *Climate response calculations*

For our analysis, we average the last 100 years of the CESM2 PI PPE and the CO_2 ensemble to remove internal variability. Since the HadCM3C PPEs have transient forcings, we averaged the last 50 years to capture the climate state at higher forcing levels. We used monthly output variables in our analysis and perform linear regressions across each set of simulations (PPE or CO_2 ensemble) to quantify the climate response per unit global-mean warming. Statistical significance is calculated using a two-tailed t test, and p values must then pass a false discovery rate of 0.05 for the gridpoint regressions (Wilks 2016).

3. Derivation of precipitation change scaling relationships

a. *Precipitation change from a moisture budget*

To understand the mechanisms contributing to land precipitation changes in the CESM2 PI PPE simulations, we analyze the steady-state atmospheric moisture budget, expressed as

$$P = E - \nabla \cdot \mathbf{F}, \tag{1}$$

where P is the precipitation, E is the ET, $\nabla\cdot$ is the two-dimensional horizontal divergence operator, and $\mathbf{F}$ is the vertically integrated horizontal moisture flux. The change in precipitation, δP, for each simulation is, therefore, given by

$$\delta P = \delta E - \delta(\nabla \cdot \mathbf{F}). \tag{2}$$

In this framework, δE can be interpreted as a direct consequence of the parameter perturbations (i.e., ET changes) in the PPEs, while $\delta(\nabla \cdot \mathbf{F})$ arises from the climate response to the parameter perturbations. Following previous studies (e.g., Held and Soden 2006; Seager et al. 2010; Boos 2012; Byrne and O'Gorman 2015; Siler et al. 2023), we decompose $\delta(\nabla \cdot \mathbf{F})$ into thermodynamic and dynamic terms (see the appendix for full derivation) which yields the scaling for δP:

$$\begin{aligned}\delta P \approx \quad & \delta E + \underbrace{\alpha_s \delta T_s (P - E)}_{\text{term 1}} + \underbrace{\left(\frac{\delta \mathcal{H}_s}{\mathcal{H}_s}\right)(P - E)}_{\text{term 2}} \\ & - \underbrace{\mathbf{F} \cdot \nabla(\alpha_s \delta T_s)}_{\text{term 3}} - \underbrace{\mathbf{F} \cdot \nabla\left(\frac{\delta \mathcal{H}_s}{\mathcal{H}_s}\right)}_{\text{term 4}} - \underbrace{\frac{1}{g}\nabla \cdot \int_0^{p_s} q\,\delta\overline{\mathbf{u}}\,dp}_{\text{term 5}}.\end{aligned} \tag{3}$$

Term 1 represents the amplification of the vertically integrated horizontal moisture flux under the conditions of fixed relative humidity and fixed circulation, known as the "wet-gets-wetter, dry-gets-drier" component (Held and Soden 2006), where T_s is the near-surface air temperature, $\alpha_s = (L_v/R_v)/T_s^2$ is the Clausius–Clapeyron scaling factor, L_v is the latent heat of vaporization, and R_v is the gas constant for water vapor. Term 2 represents the effects of local fractional changes in relative humidity (Byrne and O'Gorman 2015), where $\mathcal{H}_s$ is the near-surface relative humidity. Terms 3 and 4 represent the effects of gradients in temperature and relative humidity changes, respectively (Boos 2012; Byrne and O'Gorman 2015; Siler et al. 2023). Term 5 additionally accounts for mean circulation changes (Siler et al. 2023). The surface wind fields were only saved at the monthly frequency, so we only include the contribution from changes in monthly mean winds ($\delta\overline{\mathbf{u}}$) and neglect that from changes in transient eddies. However, the contribution of transient eddies to the change in moisture flux under warming is generally small in the global mean on annual time scales (Siler et al. 2023). Zhou et al. (2021) also show that contribution of mean wind convergence is much greater than that of transient eddies in response to large reductions in soil moisture, though the GLACE-CMIP5 experiments in their study prescribed SSTs which likely dampened large-scale shifts in circulation. Given these prior studies, we do not expect the omission of transient eddies to have a significant effect on our scaling at the global-average level.

Variations in this scaling have been used extensively to explain changes to $P - E$ under warming, and we do not derive these terms for the first time. However, the scaling provides a useful diagnosis of the relative contributions of these thermodynamic and dynamic mechanisms to moisture convergence over land. Each term in Eq. (3) is computed from climatological monthly mean model output at each grid point. Insufficient output variables from the HadCM3 PPE limited our analysis of decomposing $\nabla \cdot \mathbf{F}$ to the CESM2 PI PPE. Note that properly calculating $\mathbf{F}$ requires instantaneous, 6-hourly output to capture the transient eddy covariance terms. Because our PPE simulations only include monthly mean variables, we instead estimate $\mathbf{F}$ using 6-hourly output from the CESM2 large ensemble (Rodgers et al. 2021). Specifically, we compute $\mathbf{F}$ using output of q and $\mathbf{u}$ from the first ensemble member of the large ensemble over the period 1850–1880, which approximates preindustrial control conditions. The spatial pattern and magnitude of the calculated meridional component of $\mathbf{F}$ are similar to that in the PPE control simulation, which was fortunately saved (not shown). The zonal component of $\mathbf{F}$ in the PPE control simulation was not saved so we

Brought to you by University of Washington Libraries | Unauthenticated | Downloaded 11/20/26 03:51 PM UTC

were unable to compare it to the calculated zonal component of **F** from the CESM2 large ensemble.

b. *Tropical precipitation change from a compositing scheme*

To gain additional insight into the physical basis for precipitation change over land versus the ocean in the tropics, we use a compositing scheme developed by Lambert et al. (2017) to predict changes in tropical precipitation for 30°S–30°N. The scheme uses the weak temperature gradient approximation to link precipitation to local temperature and near-surface relative humidity anomalies relative to the tropical mean and states:

$$P_T = R(\mathcal{H}_s, T_s)\overline{P}_T, \tag{4}$$

where P_T is the tropical gridpoint precipitation, $\overline{P}_T$ is the tropical-mean precipitation, and R is a ranking function that expresses the competition for convective precipitation that is approximated as being governed by $\mathcal{H}_s$ and T_s. We modify the compositing scheme to predict tropical land-mean precipitation change. First, we assume that $R(\mathcal{H}_s, T_s)$ can be approximated as $R^*(\mathcal{H}_s)$. We justify this assumption through three lines of reasoning: 1) Lambert et al. (2017) found that land–ocean precipitation shifts are more sensitive to changes in $\mathcal{H}_s$ rank than changes in T_s rank in CMIP5 climate models, 2) variations in $\mathcal{H}_s$ are much greater than variations in T_s across the PPEs, and 3) $\mathcal{H}_s$ and T_s tend to change together. Second, we assume that tropical ocean-mean precipitation controls total tropical-mean precipitation. Applying these assumptions to Eq. (4) leaves

$$P_T = R^*(\mathcal{H}_s)\overline{P}_O, \tag{5}$$

where $\overline{P}_O$ is the tropical ocean-mean precipitation. Finally, we replace gridpoint P_T with land-mean precipitation which then allows us to linearize Eq. (5) as a function of the land–ocean contrast in $\mathcal{H}_s$:

$$\overline{P}_L \approx [a_1 + a_2(\overline{\mathcal{H}}_{s,L} - \overline{\mathcal{H}}_{s,O})]\overline{P}_O, \tag{6}$$

where $\overline{P}_L$ is the tropical land-mean precipitation, $\overline{\mathcal{H}}_{s,L}$ is the tropical land-mean relative humidity, and $\overline{\mathcal{H}}_{s,O}$ is the tropical ocean-mean relative humidity. The coefficients a_1 and a_2 are estimated through regression across each PPE (Table S4, Fig. S9). Taking the perturbation of P_L yields

$$\delta\overline{P}_L \approx a_1\delta\overline{P}_O + a_2\delta[(\overline{\mathcal{H}}_{s,L} - \overline{\mathcal{H}}_{s,O})\overline{P}_O]. \tag{7}$$

Hereafter, we call this the "full" form of precipitation change from a compositing approach. In the PPEs, we find that the change in precipitation over the ocean is quite small (Fig. 1e) such that $\delta\overline{P}_O \approx 0$ which allows us to further simplify the scaling, leaving

$$\delta\overline{P}_L \approx a_2\overline{P}_O(\delta\overline{\mathcal{H}}_{s,L} - \delta\overline{\mathcal{H}}_{s,O}). \tag{8}$$

In this "approximate" form, we can now clearly compare the relative contributions of changes in tropical $\mathcal{H}_s$ over land versus the ocean to changes in tropical land-mean precipitation. The $\delta\overline{\mathcal{H}}_{s,O}$ is relatively small (Schneider et al. 2010), so the first term in Eq. (8) dominates the response. Compared to the diagnostic moisture budget scaling, this compositing approach parameterizes all atmospheric processes, including evaporation, as responding through $\mathcal{H}_s$ which isolates the primary control of $\mathcal{H}_s$ on tropical land-mean precipitation change.

4. Results and discussion

a. *Warming driven by CO_2 versus ET*

We begin by evaluating how parameter-driven changes in evaporation relate to corresponding changes in near-surface air temperature averaged over each PPE. Over land, both the CESM2 PI and HadCM3C PPEs exhibit a strong negative correlation between ET and temperature changes ($r < -0.75$; Fig. 1a). This negative correlation is expected from the large body of literature on the influence of land surface processes on temperature (e.g., Shukla and Mintz 1982). Conversely, in the CO_2 ensemble, where climate change is driven by radiative forcing, the land-mean ET–temperature relationship has a strong positive correlation ($r = 0.96$; Fig. 1a). Both the PPEs and CO_2 ensemble have a positive correlation between ocean-mean evaporation and ocean-mean near-surface air temperature, each with approximately the same slope except for the HadCM3C Hist PPE which does not have a statistically significant relationship (Fig. 1b).

The opposite response of this temperature–ET relationship over land in the PPEs compared to the CO_2 ensemble can be explained by the different processes of radiation and ET in affecting warming. In the CO_2 ensemble, a variety of processes compete to control terrestrial ET in response to increased CO_2 and associated warming. Enhanced downward longwave radiation from higher CO_2 drives greater terrestrial evaporation, as long as there is sufficient soil moisture, by increasing the energy available to evaporate surface water and increasing the atmospheric demand for water by raising the saturation vapor pressure via warming. Changes to precipitation patterns also alter the surface water supply, influencing ET and aridity over land (e.g., Koster et al. 2004; Greve et al. 2014; Zhou et al. 2026; Lesk and Mankin 2026). In moisture-limited regions, enhancements to precipitation would increase ET while reductions would decrease ET (Budyko 1974). At the same time, the physiological effect may reduce transpiration due to stomatal closure or increase transpiration due to leaf growth fertilized by higher CO_2 levels. Stomatal closure has been shown to cause warming (Sellers et al. 1996), but the overall ET response to higher CO_2 levels is relatively uncertain due to these competing plant effects (Zarakas et al. 2020).

In contrast, parameter perturbations that alter land surface functioning and decrease terrestrial ET result in robust near-surface warming by enhancing the surface sensible heat flux. This relationship follows prior work using idealized simulations (Becker and Stevens 2014; Laguë et al. 2019, 2023) and experiments to quantify soil moisture feedbacks (Seneviratne et al. 2006, 2010; Miralles et al. 2014; Berg et al. 2016; Zhou et al. 2021) and the plant physiological effect (Sellers et al. 1996;

Brought to you by University of Washington Libraries | Unauthenticated | Downloaded 11/20/26 03:51 PM UTC

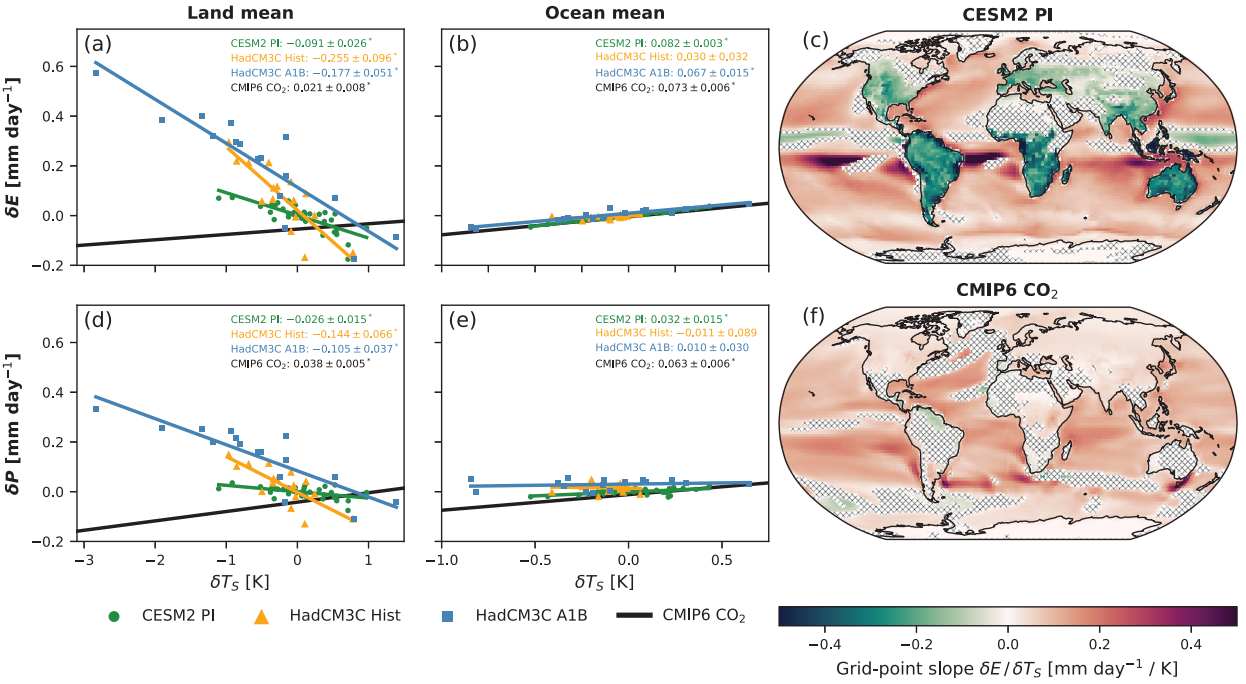

FIG. 1. The change in (a),(b) evaporation and (d),(e) precipitation plotted against the change in near-surface air temperature for each PPE. The best fit line from the total least squares (TLS) regression of the CMIP6 CO_2 experiments is shown in black. (a),(b),(d),(e) The global average over land and ocean, respectively. For each set of simulations, the slope of the TLS regression is displayed with its 95% confidence interval where an asterisk indicates $p < 0.05$ from a two-tailed t test. The slope from the gridpoint TLS regression of ET change and near-surface air temperature change across (c) the CESM2 PI PPE and (f) the CMIP6 CO_2 experiments. Hatching indicates that the slope from the gridpoint regression is not significant.

Cao et al. 2010; Arora et al. 2013, 2020; Zarakas et al. 2020). This mechanism of ET-driven temperature change follows from the construction of the surface energy budget, where net radiation into the land surface is balanced by upward latent and sensible heat fluxes as well as a downward ground heat flux into the subsurface (Monteith 1965; Bonan 2015). On the long time scales of these simulations, the ground heat flux is negligible and net downward radiation is balanced by latent and sensible heat fluxes. The same ET-driven temperature change mechanism is also observed in response to changes in plant cover or functioning including tree mortality as a result of pest infestation (Maness et al. 2013) and fire (Liu et al. 2005). It is important to note that the PPEs sample both increases and decreases in ET, and the same mechanism of warming from reduced ET works to cool the land surface when ET increases. For the remainder of the paper, we discuss our results from the perspective of decreasing ET and associated warming for simplicity, but the same relationships hold with increasing ET and associated cooling.

Unlike the ET–temperature relationship over land, evaporation over the ocean increases with both warming from reduced ET and warming from radiative forcing. In the PPEs, the ocean surface warms through advected terrestrial warming while CO_2 forcing directly warms the ocean surface via radiative processes in the CMIP6 simulations. Thus, evaporation is positively correlated with surface temperature in both cases (Siler et al. 2019).

We find that the relationships between ET and temperature are spatially coherent. The CESM2 PI PPE exhibits a distinct land–ocean contrast with a negative correlation over land, particularly in the tropics, and a positive correlation over the ocean (Fig. 1c). As expected, the presence and strength of this relationship at the gridpoint level suggests that the warming mechanism over land is primarily a local repartitioning of the surface energy budget from latent to sensible heat. Over most of the ocean surface, the positive correlation is consistent with evaporation responding to increased temperatures from advected terrestrial warming. However, in the equatorial Pacific Ocean in the CESM2 PI PPE, changes in surface wind speed from meridional shifts to the intertropical convergence zone (ITCZ) are the main control on evaporation rather than temperature (Fig. S5). In contrast, the CMIP6 CO_2 experiments have positive correlations over both land and ocean since increased surface temperature drives greater evaporation nearly everywhere (Fig. 1f).

b. *Shortwave cloud response*

In addition to the primary mechanism of warming through surface energy flux partitioning, we find that warming on land associated with reduced ET is amplified by a decrease in cloud cover. Over land, the relationship between the change in shortwave cloud radiative effect (SWCRE; defined as the shortwave cloud forcing variable in CESM2) at the top of model and the change in ET is negative in all three of the PPEs (Fig. 2). An increase in SWCRE is largely attributable to less shortwave radiation leaving the top of the atmosphere

Brought to you by University of Washington Libraries | Unauthenticated | Downloaded 11/20/26 03:51 PM UTC

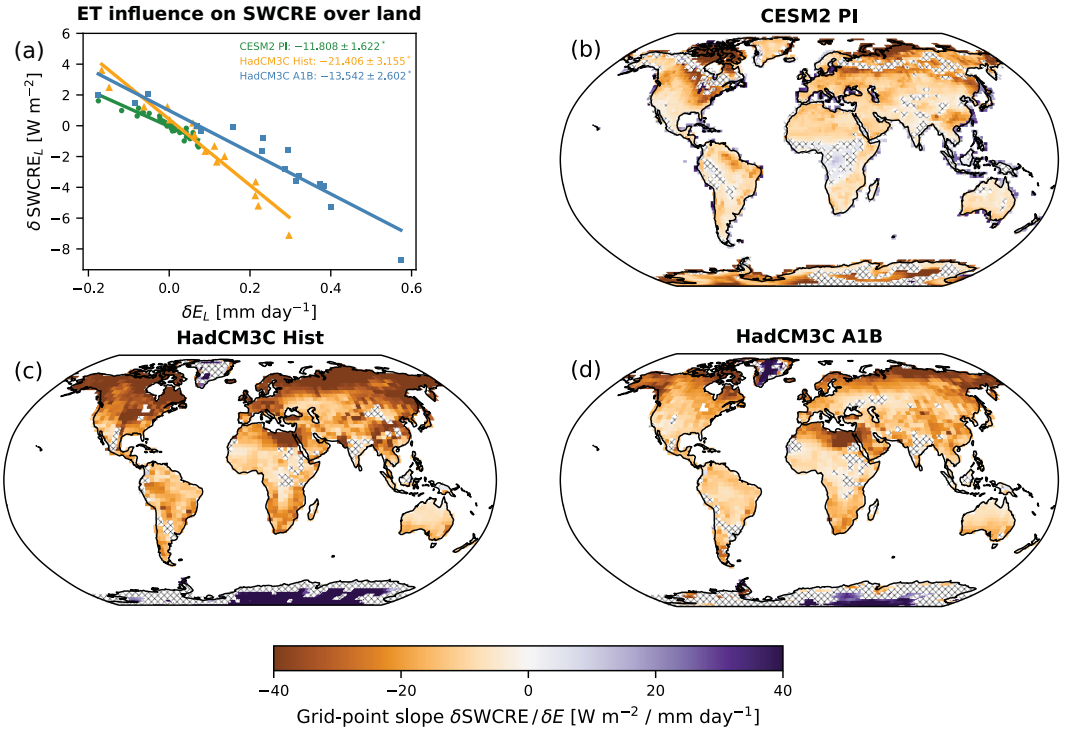

FIG. 2. The relationship between SWCRE at the top of the atmosphere and ET at the land surface. (a) The scatterplot shows the land-mean relationship with the slope from each ordinary least squares (OLS) regression in the top right and its corresponding 95% confidence interval where an asterisk indicates $p < 0.05$ from a two-tailed t test. For all PPEs, $r < -0.95$ at $p < 0.05$ using a two-tailed t test. (b)–(d) Maps show the slope of the gridpoint OLS regression where hatching indicates that the slope is not significant.

due to reduced reflection from clouds of incoming shortwave radiation which creates a net downward radiative effect, aligning with prior work (Doutriaux-Boucher et al. 2009; Andrews et al. 2011; Ban-Weiss et al. 2011; Becker and Stevens 2014; Kim et al. 2020; Laguë et al. 2023; de Vrese et al. 2024). We confirm these previous results and find a strong positive correlation between low cloud cover below 700 hPa and ET in the CESM2 PI PPE (Fig. S6), indicating that low cloud cover primarily controls the SWCRE. While cloud-cover output was not available for the HadCM3C PPE, the positive correlation between SWCRE and ET suggests that reduced ET decreases reflective cloud cover in the HadCM3C model as well.

As low cloud cover decreases with decreasing ET, more shortwave radiation reaches the land surface which further warms the land. Although the cloud parameterization schemes for our two climate models differ, with the CMIP3-era HadCM3C being significantly older than the CMIP6-era CESM2, the two versions of the HadCM3C PPE also display this negative correlation between SWCRE and ET over land indicating a consistent shortwave cloud response to relatively small ET perturbations. Thus, changes to ecosystem functioning or the ecosystem response to climate change within the range of terrestrial parametric uncertainty is likely to directly influence low clouds and the shortwave cloud radiative effect with potentially significant impacts on the top-of-the-atmosphere energy budget in global climate models. Nevertheless, low clouds represent one of the most consequential and poorly constrained components of global climate models. Low cloud feedbacks are the dominant source of intermodel spread in equilibrium climate sensitivity (Vial et al. 2013; Sherwood et al. 2014, 2020; Zelinka et al. 2020) and still have meaningful biases in climate models (Ceppi et al. 2024). Future work using large-eddy simulations or storm-resolving models to explicitly resolve the interactions between the land surface, boundary layer, and clouds under systematically varied ET would be necessary to robustly bracket the plausible range of this ET–low cloud feedback.

c. *Precipitation change over land*

To understand why land-mean precipitation responds differently to warming from ET perturbations than to warming from radiative forcing from CO_2, we analyze the atmospheric moisture budget over land and its thermodynamic and dynamic controls. We begin by contrasting changes in net moisture convergence, defined as precipitation minus evaporation ($P - E$), between the PPEs and the CO_2 ensemble. We then use the moisture budget scaling to quantify how circulation, thermodynamic factors, and relative humidity contribute to the land precipitation response (see section 3a). Finally, we assess how changes in relative humidity can act as a proxy for tropical land precipitation change using the compositing approach (see section 3b). These two approaches reveal that relative humidity, rather than moisture convergence, is tightly

Brought to you by University of Washington Libraries | Unauthenticated | Downloaded 11/20/26 03:51 PM UTC

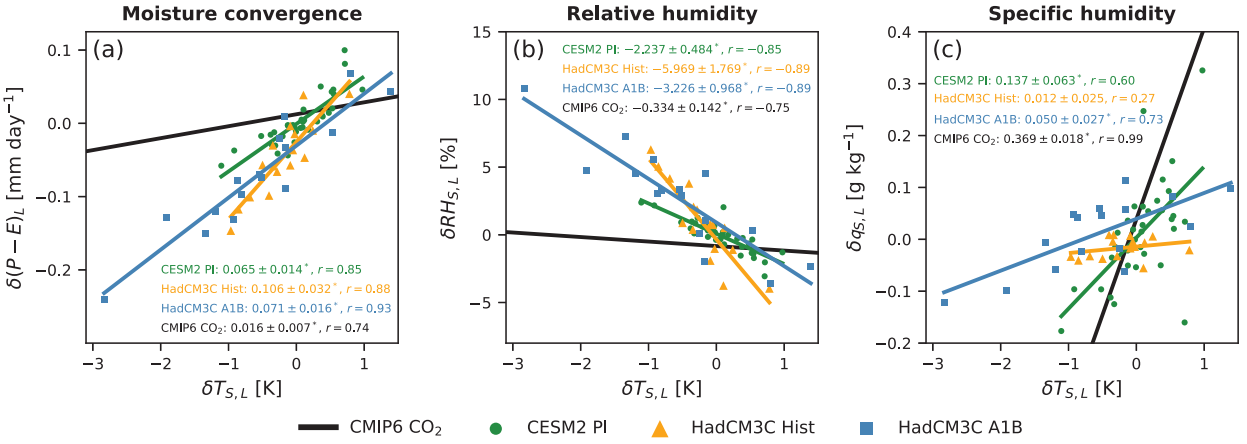

FIG. 3. The land-mean (a) change in moisture convergence computed as precipitation minus evaporation, (b) change in near-surface relative humidity, and (c) change in specific humidity plotted against the land-mean change in near-surface air temperature for each ensemble. The best fit line from the OLS regression of the CMIP6 CO_2 experiments is shown in black. The slope from each regression is displayed with its 95% confidence interval where an asterisk indicates $p < 0.05$ from a two-tailed t test. The correlation (r) is also shown.

linked to ET perturbations and the resulting precipitation response. These relationships hold over land, and the tropical precipitation scaling provides theoretical insight for the tropics.

1) MOISTURE CONVERGENCE

We find that the increase in moisture convergence per unit warming is greater in the PPEs than the CO_2 ensemble. The PPEs exhibit an increase in moisture convergence over land of 0.065–0.106 mm day^{-1} K^{-1} of land warming, while moisture convergence in the CO_2 ensemble increases at 0.016 mm day^{-1} K^{-1} (Fig. 3a). Figure 4 displays the slope from the linear regression of the actual simulated against the predicted change in moisture convergence over land from the moisture budget scaling [Eq. (3)] in the CESM2 PI PPE. We find that large-scale changes to circulation have the largest contribution to moisture convergence over land (Fig. 4, Term 5). These large-scale circulation changes primarily manifest as shifts in the ITCZ over land. As a result of the hemispherically asymmetric continental configuration, warming on land creates an interhemispheric temperature gradient causing the ITCZ to migrate toward the warmer hemisphere (Laguë et al. 2021). Unlike prior work using the GLACE experiments (e.g., Berg et al. 2016; Zhou et al. 2021), SSTs are not prescribed in the PPEs which allows for greater changes to large-scale circulation. Still, these results largely confirm the prior work from Zhou et al. (2021), which found that circulation changes drive greater moisture convergence over dry lands in response to reductions in ET from reduced soil moisture. Here, we extend their findings to globally averaged land across lower magnitude ET perturbations within the range of terrestrial parametric uncertainty and independent of land surface pathway. To the second order, thermodynamic changes via surface warming (term 1) and gradients of changes in relative humidity (term 4) both strongly correlate with moisture convergence, while local changes in relative humidity (term 2) and gradients of surface temperature (term 3) do not have any explanatory power for moisture convergence. Thus, primarily as a result of circulation changes and shifts in tropical precipitation, the PPEs have greater moisture convergence over land per degree of warming relative to the CO_2 ensemble (Fig. 3a).

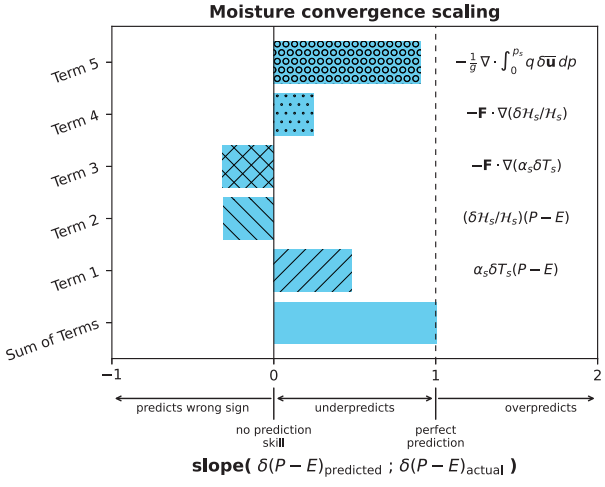

FIG. 4. The performance of the moisture convergence scaling from terms 1 to 5 in Eq. (3) for the CESM2 PI PPE plotted as the slope from the OLS regression of predicted $\delta(P-E)$ and actual simulated $\delta(P-E)$ over land.

2) PRECIPITATION RESPONSE

As in prior studies, we find that precipitation increases with temperature over both land and ocean when CO_2 concentrations are abruptly increased in the CO_2 ensemble (Figs. 1d,e; Allen and Ingram 2002; Held and Soden 2006; Fläschner et al. 2016; Pendergrass 2020; Allan et al. 2020). Over the ocean, the CESM2 PI PPE exhibits a positive correlation where surface warming induced by parameter perturbations is associated with greater precipitation, while the HadCM3C Hist and A1B PPEs have no significant relationship between surface warming and precipitation change over the ocean (Fig. 1e).

Brought to you by University of Washington Libraries | Unauthenticated | Downloaded 11/20/26 03:51 PM UTC

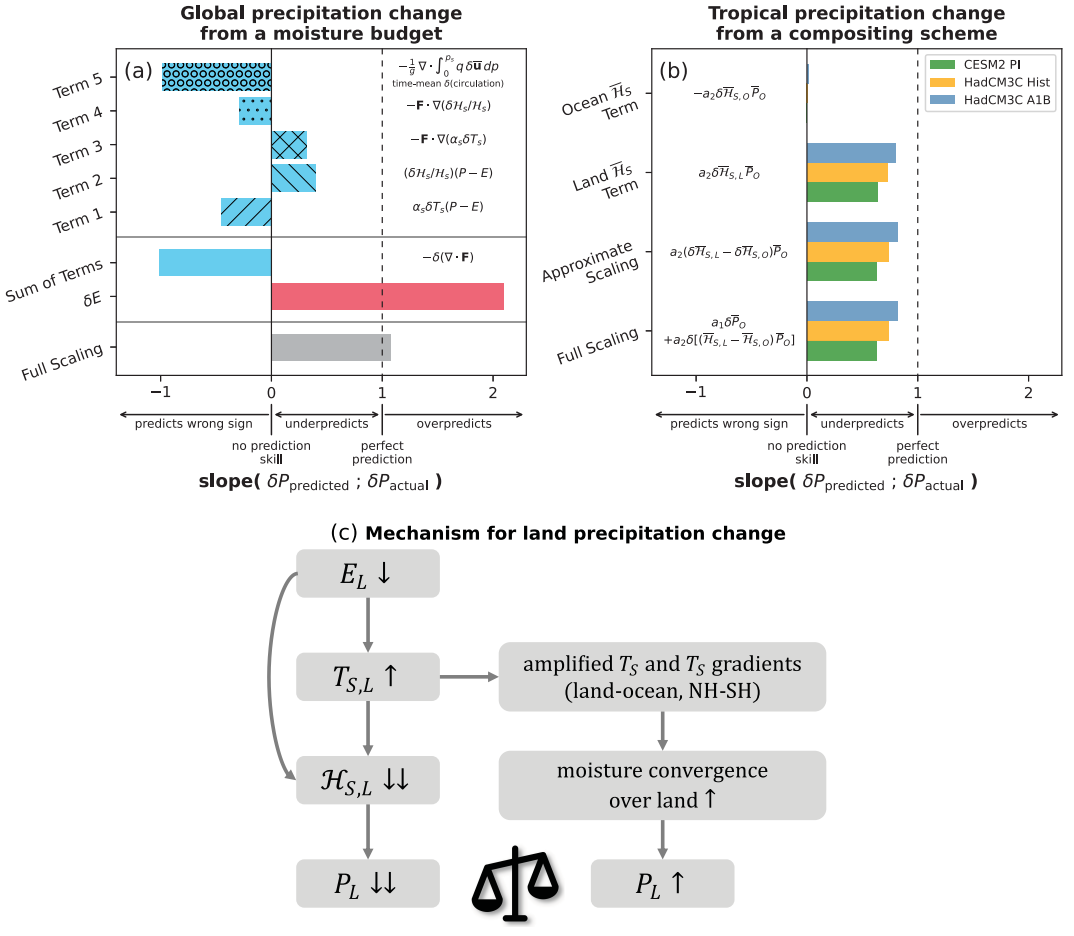

FIG. 5. The performance of (a) the moisture budget scaling from Eq. (3) for the CESM2 PI PPE and (b) the tropical precipitation scaling from Eqs. (7) and (8) each plotted as the slope from the OLS regression of predicted δP and actual simulated δP over land. The tropical precipitation scaling is only applied to tropical precipitation change. (c) A conceptual diagram of the mechanism for land precipitation change.

As was the case for ET, the PPEs exhibit an opposite response of precipitation to warming over land versus over the ocean. In response to ET forcing, land-mean precipitation changes are negatively correlated with land-mean temperature changes such that surface warming is associated with reduced precipitation (Fig. 1d). The surface warming and decline in precipitation are consequences of the reduced ET. The opposite behavior of land-mean precipitation with warming in the PPEs relative to the CO_2 ensemble suggests that a different set of mechanisms drives land-mean precipitation changes in response to terrestrial ET perturbations. While these PPE results hold for two different climate models, the coarse horizontal model resolution may limit the fidelity of simulated precipitation and land–atmosphere feedbacks (Stephens et al. 2010; Chen and Dai 2019; Lee and Hohenegger 2024).

To explain the land-mean precipitation response to ET perturbations versus radiative forcing from CO_2, we identify changes to moisture convergence and near-surface relative humidity as the key controls. First, we find that moisture convergence in the CESM2 PI PPE (Fig. 5a; sum of terms) predicts the wrong sign of precipitation change. The moisture budget scaling reveals that the contribution to precipitation change from ET is double the contribution from moisture convergence and dominates the precipitation response (Fig. 5a). For the CESM2 PI PPE, where ET is the main driver of warming, these results indicate that moisture convergence increases mainly due to circulation shifts and higher moisture content associated with ET-driven warming (Fig. 5a; term 1, term 5, and sum of terms). Although this increase would typically enhance precipitation, the reduction in ET (Fig. 5a; δE) dominates, leading to decreased precipitation over land.

While we focus on land-mean change, Pietschnig et al. (2021) find that the effect of moisture largely depends on the width of the continent, determining whether increased moisture convergence or decreased local moisture supply dominates the precipitation response to reduced ET. Over narrower continents, increased moisture convergence over land dominates and precipitation increases, while over wider continents, local reductions in ET dominate and precipitation decreases. Our results indicate that in the land mean, ET overwhelms the increased moisture convergence.

However, even with decreased ET, specific humidity increases with warming across the PPEs, though the relationship is weak

Brought to you by University of Washington Libraries | Unauthenticated | Downloaded 11/20/26 03:51 PM UTC

due to the competition between increased moisture convergence and decreased ET over land (Fig. 3c). This suggests that the decline in absolute moisture from ET is unlikely to be the sole driver of decreased precipitation. Instead, we turn to prior work showing that precipitation in the time mean is associated with higher near-surface relative humidity (Chadwick et al. 2013; Lambert et al. 2017; Fan et al. 2021; Cheng et al. 2021; van der Drift and O'Gorman 2025). In other words, greater moisture alone will not enhance precipitation if the moisture does not condense. Even though there is greater moisture convergence over land and no coherent change in specific humidity with warming, the PPEs have a greater decrease in relative humidity per degree warming than the CO_2 ensemble due to direct reductions in ET (Fig. 3b). We partition the change in relative humidity into contributions from temperature and specific humidity and find that warming primarily drives the decrease in relative humidity (Fig. S7). Changes to moisture actually contribute a small increase in relative humidity, suggesting that greater imported moisture from the ocean overcomes the lower surface moisture flux from reduced ET (Fig. S7).

The strong control of ET on relative humidity in the PPEs aligns with land climate theory. Byrne and O'Gorman (2016) theorized that nonradiative moisture forcings over land (i.e., from ET) could initiate a feedback to amplify decreases in land relative humidity, primarily through warming, and intensify the land–ocean temperature gradient. More recently, McColl and Tang (2024) developed a simple theory that describes relative humidity over land as a function of only the evaporative fraction, asserting that the partitioning of ET and sensible heat is the primary control of relative humidity. Our results broadly confirm these theories in complex Earth system models and show that changes in ET within the range of parametric uncertainty can play an important role in modulating land relative humidity.

The tropical compositing approach in Eq. (7) provides a complementary perspective for understanding tropical precipitation change by using relative humidity to parameterize precipitation. The theoretical underpinnings of the scaling depend on the weak temperature gradient approximation, which limits its application to the tropics. Conceptually, this approach assumes that tropical humidity, temperature, and moisture convergence change together in a consistent way across different simulations from the same model. We fit a relationship between tropical relative humidity and precipitation to the control simulation [Eq. (6)] and use that relationship to predict changes in tropical precipitation across the PPE. Applying the compositing approach from Eq. (7) in each PPE, we find that the change in land precipitation is well predicted by the change in land relative humidity scaled by ocean precipitation from the control simulation for the tropics (Fig. 5b; full scaling). As expected, tropical relative humidity over the ocean remains nearly constant and has no predictive power such that the term containing the change in tropical land relative humidity and the control tropical ocean-mean precipitation has equal predictive skill to the full compositing approach (Fig. 5b; land $\overline{\mathcal{H}}_S$ term). The skill of this simple compositing approach reveals the central role of land relative humidity in controlling land precipitation in response to ET perturbations in the tropics. In other words, the significant decrease in relative humidity caused by reductions in ET and associated warming can explain the decrease in land precipitation in the PPEs, whereas the modest decrease in relative humidity from radiative forcing in the CO_2 ensemble is not large enough to exert control on precipitation. Interestingly, the compositing approach also works in the global mean (Fig. S8) even though the compositing scheme from Lambert et al. (2017) was derived for the tropics, and further work is needed to understand why this is. Conceptually, this compositing approach should provide skill in predicting the response across simulations of many types for a given model, not just the PPEs. We performed the same regression to compute the a_2 coefficient in Eq. (7) for each CMIP6 model in the CO_2 ensemble. However, the a_2 coefficient varied significantly across the CO_2 ensemble, and the compositing approach was completely unable to predict land precipitation change for some models (Fig. S9b, Table S4).

5. Conclusions and implications

In this study, we use a unique set of perturbed parameter ensembles from CESM2 and HadCM3C to investigate the sensitivity of the global hydrological cycle to warming driven by changes in land surface conditions. We find that decreasing ET warms the land surface and reduces land-mean precipitation, opposite to the increase in precipitation with warming from CO_2 forcing. Consistent with previous studies, reductions in ET are associated with a robust warming response (e.g., Shukla and Mintz 1982) which is amplified by a shortwave cloud feedback (Doutriaux-Boucher et al. 2009; Kim et al. 2020; Laguë et al. 2023; de Vrese et al. 2024). While the representation of clouds in climate models remains highly uncertain, our results uniquely display this mechanism across two models with different cloud parameterization schemes and across small ET perturbations. The decrease in land-mean precipitation occurs despite increases in moisture convergence associated with land warming. Our results extend prior work (Berg et al. 2016; Zhou et al. 2021) to smaller ET perturbations within the range of terrestrial uncertainty and agnostic of land surface process while directly contrasting the precipitation response over land to the robust increase in precipitation with warming from radiative forcing. Reduced ET significantly decreases land relative humidity per unit warming while also increasing specific humidity and moisture convergence over land per unit warming by shifting large-scale circulation. We hypothesize that the decrease in land-mean relative humidity, and the land–ocean relative humidity gradient it produces, drives the decrease in precipitation. In the tropics, scaling ocean-mean precipitation with land–ocean gradients in relative humidity well captures the land-mean precipitation change simulated in the PPEs, though the theoretical basis of the scaling relies on the weak temperature gradient approximation which limits its application to the tropics. While we only analyzed two climate models with relatively coarse resolution, our results suggest that changes to land surface properties at the magnitude of terrestrial parametric uncertainty influence ET and drive large-scale precipitation changes and a positive shortwave cloud feedback.

Brought to you by University of Washington Libraries | Unauthenticated | Downloaded 11/20/26 03:51 PM UTC

Our results have implications for projecting and attributing precipitation changes under a changing climate. Future climate will reflect the combined influence of radiative forcing from increases in greenhouse gases and nonradiative land surface changes arising from human-caused land-use change and plant physiological responses to elevated CO_2. While radiatively forced warming from greenhouse gases has been shown by many prior studies to increase precipitation over land broadly, our findings demonstrate that warming driven by reductions in ET due to uncertainty in land processes can oppose this tendency, decreasing precipitation over land and potentially moderating the rate of global precipitation increase while also contributing to terrestrial warming.

Acknowledgments. B. G. B. and A. L. S. S. were supported by National Science Foundation (NSF) Awards DEB-1925837 and AWD-022757. F. H. L. was partly supported by Natural Environment Research Council CIRCULATES (NE/T006285/1). D. B. B. was supported by the Cooperative Institute for Climate, Ocean, and Ecosystem Studies (CICOES) under NOAA Cooperative Agreement NA20OAR4320271, Contribution 2025-1509. The CESM project is supported primarily by the NSF. This material is based upon work supported by the NSF National Center for Atmospheric Research (NCAR), which is a major facility sponsored by the NSF under Cooperative Agreement 1852977. Computing and data storage resources, including the Cheyenne (https://doi.org/10.5065/D6RX99HX) and Derecho (https://doi.org/10.5065/qx9a-pg09) systems, were provided by the Computational and Information Systems Laboratory (CISL) at NSF NCAR. We thank all the scientists, software engineers, and administrators who contributed to the development of CESM2.

Data availability statement. All analysis scripts are available at Buchovecky (2025). Model output necessary to generate the main figures and all perturbed parameter files for the CESM2 PI PPE are available on Dryad at Buchovecky et al. (2026).

APPENDIX

Derivation of Precipitation Change Scaling from a Moisture Budget

To decompose $\delta(\nabla\cdot\mathbf{F})$ into thermodynamic and dynamic terms, we first express specific humidity as $q=\mathcal{H}q^*$, where q^* is the saturation specific humidity and $\mathcal{H}$ is the relative humidity. The linearized fractional change in q can then be written as

$$\frac{\delta q}{q}\approx\left(\frac{\delta q^*}{q^*}+\frac{\delta\mathcal{H}}{\mathcal{H}}\right). \tag{A1}$$

In line with prior work (i.e., Held and Soden 2006; Boos 2012; Byrne and O'Gorman 2015), we assume that variations in each term are dominated by near-surface changes, so Eq. (A1) becomes

$$\delta q\approx\left(\alpha_s\delta T_s+\frac{\delta\mathcal{H}_s}{\mathcal{H}_s}\right)q, \tag{A2}$$

where $\alpha_s=(L_v/R_v)/T_s^2$ is the Clausius–Clapeyron scaling factor, L_v is the latent heat of vaporization, R_v is the gas constant for water vapor, $\mathcal{H}_s$ is the near-surface relative humidity, and T_s is the near-surface temperature. We apply δq from Eq. (A1) to $\delta\mathbf{F}$ with no change in $\mathbf{u}$, resulting in

$$\delta\mathbf{F}_q\approx\frac{1}{g}\int_0^{p_s}\left(\alpha_s\delta T_s+\frac{\delta\mathcal{H}_s}{\mathcal{H}_s}\right)q\mathbf{u}dp=\left(\alpha_s\delta T_s+\frac{\delta\mathcal{H}_s}{\mathcal{H}_s}\right)\mathbf{F}. \tag{A3}$$

Taking the divergence of Eq. (A3), applying the product rule, and using Eq. (1) to simplify yield the full thermodynamic contribution:

$$-\delta(\nabla\cdot\mathbf{F})_q\approx\alpha_s\delta T_s(P-E)+\left(\frac{\delta\mathcal{H}_s}{\mathcal{H}_s}\right)(P-E)-\mathbf{F}\cdot\nabla(\alpha_s\delta T_s)-\mathbf{F}\cdot\nabla\left(\frac{\delta\mathcal{H}_s}{\mathcal{H}_s}\right). \tag{A4}$$

Perturbations to land surface processes can also strongly influence the mean atmospheric circulation (e.g., Laguë and Swann 2016; Kooperman et al. 2018; Laguë et al. 2019, 2021), producing a dynamic contribution to $\delta(\nabla\cdot\mathbf{F})$. The dynamic contribution is quantified through changes in the mean circulation ($\delta\overline{\mathbf{u}}$) holding q constant, which we calculate as

$$-\delta(\nabla\cdot\mathbf{F})_u\approx-\frac{1}{g}\nabla\cdot\int_0^{p_s}q\,\delta\overline{\mathbf{u}}dp, \tag{A5}$$

where $\delta\overline{\mathbf{u}}$ denotes the change in monthly mean winds. We did not have submonthly surface wind fields to compute the transient eddies contribution, but the contribution of transient eddies to the change in moisture flux under warming is generally small over global land (Siler et al. 2023). Using simulations with fixed SSTs, Zhou et al. (2021) additionally show that contribution of mean wind convergence is much greater than that of transient eddies in response to large reductions in soil moisture. Combining Eqs. (A4) and. (A5) with Eq. (2) yields our full scaling for δP:

$$\delta P\approx\delta E+\underbrace{\alpha_s\delta T_s(P-E)}_{\text{term 1}}+\underbrace{\left(\frac{\delta\mathcal{H}_s}{\mathcal{H}_s}\right)(P-E)}_{\text{term 2}}-\underbrace{\mathbf{F}\cdot\nabla(\alpha_s\delta T_s)}_{\text{term 3}}-\underbrace{\mathbf{F}\cdot\nabla\left(\frac{\delta\mathcal{H}_s}{\mathcal{H}_s}\right)}_{\text{term 4}}-\underbrace{\frac{1}{g}\nabla\cdot\int_0^{p_s}q\,\delta\overline{\mathbf{u}}dp}_{\text{term 5}}. \tag{A6}$$

REFERENCES

Allan, R. P., and Coauthors, 2020: Advances in understanding large-scale responses of the water cycle to climate change. *Ann. N. Y. Acad. Sci.*, **1472**, 49–75, https://doi.org/10.1111/nyas.14337.

Allen, M. R., and W. J. Ingram, 2002: Constraints on future changes in climate and the hydrologic cycle. *Nature*, **419**, 224–232, https://doi.org/10.1038/nature01092.

Andrews, T., M. Doutriaux-Boucher, O. Boucher, and P. M. Forster, 2011: A regional and global analysis of carbon

Brought to you by University of Washington Libraries | Unauthenticated | Downloaded 11/20/26 03:51 PM UTC

dioxide physiological forcing and its impact on climate. *Climate Dyn.*, **36**, 783–792, https://doi.org/10.1007/s00382-010-0742-1.

Arora, V. K., and Coauthors, 2013: Carbon–concentration and carbon–climate feedbacks in CMIP5 Earth system models. *J. Climate*, **26**, 5289–5314, https://doi.org/10.1175/JCLI-D-12-00494.1.

——, and Coauthors, 2020: Carbon–concentration and carbon–climate feedbacks in CMIP6 models and their comparison to CMIP5 models. *Biogeosciences*, **17**, 4173–4222, https://doi.org/10.5194/bg-17-4173-2020.

Ban-Weiss, G. A., G. Bala, L. Cao, J. Pongratz, and K. Caldeira, 2011: Climate forcing and response to idealized changes in surface latent and sensible heat. *Environ. Res. Lett.*, **6**, 034032, https://doi.org/10.1088/1748-9326/6/3/034032.

Becker, T., and B. Stevens, 2014: Climate and climate sensitivity to changing CO_2 on an idealized land planet. *J. Adv. Model. Earth Syst.*, **6**, 1205–1223, https://doi.org/10.1002/2014MS000369.

Berg, A., and J. Sheffield, 2018: Soil moisture–evapotranspiration coupling in CMIP5 models: Relationship with simulated climate and projections. *J. Climate*, **31**, 4865–4878, https://doi.org/10.1175/JCLI-D-17-0757.1.

——, and Coauthors, 2016: Land–atmosphere feedbacks amplify aridity increase over land under global warming. *Nat. Climate Change*, **6**, 869–874, https://doi.org/10.1038/nclimate3029.

Betts, R. A., P. M. Cox, S. E. Lee, and F. I. Woodward, 1997: Contrasting physiological and structural vegetation feedbacks in climate change simulations. *Nature*, **387**, 796–799, https://doi.org/10.1038/42924.

——, and Coauthors, 2007: Projected increase in continental runoff due to plant responses to increasing carbon dioxide. *Nature*, **448**, 1037–1041, https://doi.org/10.1038/nature06045.

Bogenschutz, P. A., A. Gettelman, C. Hannay, V. E. Larson, R. B. Neale, C. Craig, and C.-C. Chen, 2018: The path to CAM6: Coupled simulations with CAM5.4 and CAM5.5. *Geosci. Model Dev.*, **11**, 235–255, https://doi.org/10.5194/gmd-11-235-2018.

Bonan, G., 2015: *Ecological Climatology: Concepts and Applications.* 3rd ed. Cambridge University Press, 692 pp., https://doi.org/10.1017/CBO9781107339200.

Bony, S., G. Bellon, D. Klocke, S. Sherwood, S. Fermepin, and S. Denvil, 2013: Robust direct effect of carbon dioxide on tropical circulation and regional precipitation. *Nat. Geosci.*, **6**, 447–451, https://doi.org/10.1038/ngeo1799.

Boos, W. R., 2012: Thermodynamic scaling of the hydrological cycle of the last glacial maximum. *J. Climate*, **25**, 992–1006, https://doi.org/10.1175/JCLI-D-11-00010.1.

Booth, B. B. B., and Coauthors, 2012: High sensitivity of future global warming to land carbon cycle processes. *Environ. Res. Lett.*, **7**, 024002, https://doi.org/10.1088/1748-9326/7/2/024002.

Buchovecky, B. G., 2025: bbuchovecky/et_precip_ppe: Et_precip_ppe. Zenodo, https://doi.org/10.5281/zenodo.17945232.

——, F. H. Lambert, C. M. Zarakas, M. M. Laguë, C. D. Koven, I. Y. Fung, D. B. Bonan, and A. L. S. Swann, 2026: Data from: "Reduced evapotranspiration decreases land precipitation despite enhanced moisture convergence: Insights from perturbed parameter ensembles of Earth system models". Dryad, accessed 17 June 2026, https://doi.org/10.5061/dryad.8kprr4z23.

Budyko, M. I., 1974: *Climate and Life.* International Gephysics Series, Vol. 18, Academic Press, 507 pp.

Byrne, M. P., and P. A. O'Gorman, 2015: The response of precipitation minus evapotranspiration to climate warming: Why the "wet-get-wetter, dry-get-drier" scaling does not hold over land. *J. Climate*, **28**, 8078–8092, https://doi.org/10.1175/JCLI-D-15-0369.1.

——, and ——, 2016: Understanding decreases in land relative humidity with global warming: Conceptual model and GCM simulations. *J. Climate*, **29**, 9045–9061, https://doi.org/10.1175/JCLI-D-16-0351.1.

Cao, L., G. Bala, K. Caldeira, R. Nemani, and G. Ban-Weiss, 2010: Importance of carbon dioxide physiological forcing to future climate change. *Proc. Natl. Acad. Sci. USA*, **107**, 9513–9518, https://doi.org/10.1073/pnas.0913000107.

Ceppi, P., T. A. Myers, P. Nowack, C. J. Wall, and M. D. Zelinka, 2024: Implications of a pervasive climate model bias for low-cloud feedback. *Geophys. Res. Lett.*, **51**, e2024GL110525, https://doi.org/10.1029/2024GL110525.

Chadwick, R., I. Boutle, and G. Martin, 2013: Spatial patterns of precipitation change in CMIP5: Why the rich do not get richer in the tropics. *J. Climate*, **26**, 3803–3822, https://doi.org/10.1175/JCLI-D-12-00543.1.

——, D. Ackerley, T. Ogura, and D. Dommenget, 2019: Separating the influences of land warming, the direct CO_2 effect, the plant physiological effect, and SST warming on regional precipitation changes. *J. Geophys. Res. Atmos.*, **124**, 624–640, https://doi.org/10.1029/2018JD029423.

Chen, D., and A. Dai, 2019: Precipitation characteristics in the Community Atmosphere Model and their dependence on model physics and resolution. *J. Adv. Model. Earth Syst.*, **11**, 2352–2374, https://doi.org/10.1029/2018MS001536.

Cheng, Y., P. W. Chan, X. Wei, Z. Hu, Z. Kuang, and K. A. McColl, 2021: Soil moisture control of precipitation reevaporation over a heterogeneous land surface. *J. Atmos. Sci.*, **78**, 3369–3383, https://doi.org/10.1175/JAS-D-21-0059.1.

Chou, C., J. D. Neelin, C.-A. Chen, and J.-Y. Tu, 2009: Evaluating the "rich-get-richer" mechanism in tropical precipitation change under global warming. *J. Climate*, **22**, 1982–2005, https://doi.org/10.1175/2008JCLI2471.1.

Cox, P. M., 2001: Description of the "TRIFFID" dynamic global vegetation model. Met Office Hadley Centre Tech. Note 24, 17 pp., https://www.paleo.bristol.ac.uk/UM_Docs/UM_Technical_Documents/HCTN_24_TRIFFID.pdf.

——, R. A. Betts, C. D. Jones, S. A. Spall, and I. J. Totterdell, 2000: Acceleration of global warming due to carbon-cycle feedbacks in a coupled climate model. *Nature*, **408**, 184–187, https://doi.org/10.1038/35041539.

Danabasoglu, G., and P. R. Gent, 2009: Equilibrium climate sensitivity: Is it accurate to use a slab ocean model? *J. Climate*, **22**, 2494–2499, https://doi.org/10.1175/2008JCLI2596.1.

——, and Coauthors, 2020: The Community Earth System Model Version 2 (CESM2). *J. Adv. Model. Earth Syst.*, **12**, e2019MS001916, https://doi.org/10.1029/2019MS001916.

DeAngelis, A. M., X. Qu, M. D. Zelinka, and A. Hall, 2015: An observational radiative constraint on hydrologic cycle intensification. *Nature*, **528**, 249–253, https://doi.org/10.1038/nature15770.

de Vrese, P., T. Stacke, V. Gayler, and V. Brovkin, 2024: Permafrost cloud feedback may amplify climate change. *Geophys. Res. Lett.*, **51**, e2024GL109034, https://doi.org/10.1029/2024GL109034.

Doutriaux-Boucher, M., M. J. Webb, J. M. Gregory, and O. Boucher, 2009: Carbon dioxide induced stomatal closure increases radiative forcing via a rapid reduction in low cloud. *Geophys. Res. Lett.*, **36**, L02703, https://doi.org/10.1029/2008GL036273.

Brought to you by University of Washington Libraries | Unauthenticated | Downloaded 11/20/26 03:51 PM UTC

Eltahir, E. A. B., 1998: A soil moisture–rainfall feedback mechanism: 1. Theory and observations. *Water Resour. Res.*, **34**, 765–776, https://doi.org/10.1029/97WR03499.

Eyring, V., S. Bony, G. A. Meehl, C. A. Senior, B. Stevens, R. J. Stouffer, and K. E. Taylor, 2016: Overview of the Coupled Model Intercomparison Project phase 6 (CMIP6) experimental design and organization. *Geosci. Model Dev.*, **9**, 1937–1958, https://doi.org/10.5194/gmd-9-1937-2016.

Falloon, P. D., R. Dankers, R. A. Betts, C. D. Jones, B. B. B. Booth, and F. H. Lambert, 2012: Role of vegetation change in future climate under the A1B scenario and a climate stabilisation scenario, using the HadCM3C Earth system model. *Biogeosciences*, **9**, 4739–4756, https://doi.org/10.5194/bg-9-4739-2012.

Fan, B., Z. Tan, T. A. Shaw, and E. S. Kite, 2021: Reducing surface wetness leads to tropical hydrological cycle regime transition. *Geophys. Res. Lett.*, **48**, e2020GL090746, https://doi.org/10.1029/2020GL090746.

Fläschner, D., T. Mauritsen, and B. Stevens, 2016: Understanding the intermodel spread in global-mean hydrological sensitivity. *J. Climate*, **29**, 801–817, https://doi.org/10.1175/JCLI-D-15-0351.1.

Gordon, C., C. Cooper, C. A. Senior, H. Banks, J. M. Gregory, T. C. Johns, J. F. B. Mitchell, and R. A. Wood, 2000: The simulation of SST, sea ice extents and ocean heat transports in a version of the Hadley Centre coupled model without flux adjustments. *Climate Dyn.*, **16**, 147–168, https://doi.org/10.1007/s003820050010.

Greve, P., B. Orlowsky, B. Mueller, J. Sheffield, M. Reichstein, and S. I. Seneviratne, 2014: Global assessment of trends in wetting and drying over land. *Nat. Geosci.*, **7**, 848, https://doi.org/10.1038/ngeo2247.

Guo, Z., and Coauthors, 2006: GLACE: The Global Land–Atmosphere Coupling Experiment. Part II: Analysis. *J. Hydrometeor.*, **7**, 611–625, https://doi.org/10.1175/JHM511.1.

Held, I. M., and B. J. Soden, 2006: Robust responses of the hydrological cycle to global warming. *J. Climate*, **19**, 5686–5699, https://doi.org/10.1175/JCLI3990.1.

Kennedy, D., and Coauthors, 2025: One-at-a-time parameter perturbation ensemble of the Community Land Model, version 5.1. *J. Adv. Model. Earth Syst.*, **17**, e2024MS004715, https://doi.org/10.1029/2024MS004715.

Kim, J. E., M. M. Laguë, S. Pennypacker, E. Dawson, and A. L. S. Swann, 2020: Evaporative resistance is of equal importance as surface albedo in high-latitude surface temperatures due to cloud feedbacks. *Geophys. Res. Lett.*, **47**, e2019GL085663, https://doi.org/10.1029/2019GL085663.

Kooperman, G. J., M. D. Fowler, F. M. Hoffman, C. D. Koven, K. Lindsay, M. S. Pritchard, A. L. S. Swann, and J. T. Randerson, 2018: Plant physiological responses to rising CO_2 modify simulated daily runoff intensity with implications for global-scale flood risk assessment. *Geophys. Res. Lett.*, **45**, 12 457 –12 466, https://doi.org/10.1029/2018GL079901.

Koster, R. D., and Coauthors, 2004: Regions of strong coupling between soil moisture and precipitation. *Science*, **305**, 1138–1140, https://doi.org/10.1126/science.1100217.

——, and Coauthors, 2006: GLACE: The Global Land–Atmosphere Coupling Experiment. Part I: Overview. *J. Hydrometeor.*, **7**, 590–610, https://doi.org/10.1175/JHM510.1.

——, and Coauthors, 2010: Contribution of land surface initialization to subseasonal forecast skill: First results from a multimodel experiment. *Geophys. Res. Lett.*, **37**, L02402, https://doi.org/10.1029/2009GL041677.

Krakauer, N. Y., B. I. Cook, and M. J. Puma, 2010: Contribution of soil moisture feedback to hydroclimatic variability. *Hydrol. Earth Syst. Sci.*, **14**, 505–520, https://doi.org/10.5194/hess-14-505-2010.

Laguë, M. M., and A. L. S. Swann, 2016: Progressive midlatitude afforestation: Impacts on clouds, global energy transport, and precipitation. *J. Climate*, **29**, 5561–5573, https://doi.org/10.1175/JCLI-D-15-0748.1.

——, G. B. Bonan, and A. L. S. Swann, 2019: Separating the impact of individual land surface properties on the terrestrial surface energy budget in both the coupled and uncoupled land–atmosphere system. *J. Climate*, **32**, 5725–5744, https://doi.org/10.1175/JCLI-D-18-0812.1.

——, A. L. S. Swann, and W. R. Boos, 2021: Radiative feedbacks on land surface change and associated tropical precipitation shifts. *J. Climate*, **34**, 6651–6672, https://doi.org/10.1175/JCLI-D-20-0883.1.

——, G. R. Quetin, and W. R. Boos, 2023: Reduced terrestrial evaporation increases atmospheric water vapor by generating cloud feedbacks. *Environ. Res. Lett.*, **18**, 074021, https://doi.org/10.1088/1748-9326/acdbe1.

Lambert, F. H., and M. J. Webb, 2008: Dependency of global mean precipitation on surface temperature. *Geophys. Res. Lett.*, **35**, L16706, https://doi.org/10.1029/2008GL034838.

——, G. R. Harris, M. Collins, J. M. Murphy, D. M. H. Sexton, and B. B. B. Booth, 2013: Interactions between perturbations to different Earth system components simulated by a fully-coupled climate model. *Climate Dyn.*, **41**, 3055–3072, https://doi.org/10.1007/s00382-012-1618-3.

——, A. J. Ferraro, and R. Chadwick, 2017: Land–ocean shifts in tropical precipitation linked to surface temperature and humidity change. *J. Climate*, **30**, 4527–4545, https://doi.org/10.1175/JCLI-D-16-0649.1.

Langenbrunner, B., M. S. Pritchard, G. J. Kooperman, and J. T. Randerson, 2019: Why does Amazon precipitation decrease when tropical forests respond to increasing CO_2? *Earth's Future*, **7**, 450–468, https://doi.org/10.1029/2018EF001026.

Lawrence, D. M., and Coauthors, 2019: The Community Land Model version 5: Description of new features, benchmarking, and impact of forcing uncertainty. *J. Adv. Model. Earth Syst.*, **11**, 4245–4287, https://doi.org/10.1029/2018MS001583.

Lee, J., and C. Hohenegger, 2024: Weaker land–atmosphere coupling in global storm-resolving simulation. *Proc. Natl. Acad. Sci. USA*, **121**, e2314265121, https://doi.org/10.1073/pnas.2314265121.

Lesk, C. S., and J. S. Mankin, 2026: More concentrated precipitation decreases terrestrial water storage. *Nature*, **653**, 425–432, https://doi.org/10.1038/s41586-026-10487-7.

Liu, H., J. T. Randerson, J. Lindfors, and F. S. Chapin III, 2005: Changes in the surface energy budget after fire in boreal ecosystems of interior Alaska: An annual perspective. *J. Geophys. Res.*, **110**, D13101, https://doi.org/10.1029/2004JD005158.

Maness, H., P. J. Kushner, and I. Fung, 2013: Summertime climate response to mountain pine beetle disturbance in British Columbia. *Nat. Geosci.*, **6**, 65–70, https://doi.org/10.1038/ngeo1642.

Mankin, J. S., and Coauthors, 2025: Nonlinear carbon feedbacks in CMIP6 and their impacts on future freshwater availability. *J. Climate*, **38**, 3333–3352, https://doi.org/10.1175/JCLI-D-24-0028.1.

Brought to you by University of Washington Libraries | Unauthenticated | Downloaded 11/20/26 03:51 PM UTC

McColl, K. A., and L. I. Tang, 2024: An analytic theory of near-surface relative humidity over land. *J. Climate*, **37**, 1213–1230, https://doi.org/10.1175/JCLI-D-23-0342.1.

Miralles, D. G., and Coauthors, 2014: El Niño–La Niña cycle and recent trends in continental evaporation. *Nat. Climate Change*, **4**, 122–126, https://doi.org/10.1038/nclimate2068.

Monteith, J. L., 1965: Evaporation and environment. *Symp. Soc. Exp. Biol.*, **19**, 205–234.

Nakicenovic, N., R. Swart, J. Alcamo, G. Davis, B. de Vries, and J. Fenhann, 2000: *IPCC Special Report on Emissions Scenarios.* Cambridge University Press, 570 pp.

O'Gorman, P. A., R. P. Allan, M. P. Byrne, and M. Previdi, 2012: Energetic constraints on precipitation under climate change. *Surv. Geophys.*, **33**, 585–608, https://doi.org/10.1007/s10712-011-9159-6.

Pendergrass, A. G., 2020: The global-mean precipitation response to CO_2-induced warming in CMIP6 models. *Geophys. Res. Lett.*, **47**, e2020GL089964, https://doi.org/10.1029/2020GL089964.

——, and D. L. Hartmann, 2014: The atmospheric energy constraint on global-mean precipitation change. *J. Climate*, **27**, 757–768, https://doi.org/10.1175/JCLI-D-13-00163.1.

Pietschnig, M., F. H. Lambert, M. Saint-Lu, and G. K. Vallis, 2019: The presence of Africa and limited soil moisture contribute to future drying of South America. *Geophys. Res. Lett.*, **46**, 12 445–12 453, https://doi.org/10.1029/2019GL084441.

——, A. L. S. Swann, F. H. Lambert, and G. K. Vallis, 2021: Response of tropical rainfall to reduced evapotranspiration depends on continental extent. *J. Climate*, **34**, 9221–9234, https://doi.org/10.1175/JCLI-D-21-0195.1.

Pu, B., and R. E. Dickinson, 2014: Hydrological changes in the climate system from leaf responses to increasing CO_2. *Climate Dyn.*, **42**, 1905–1923, https://doi.org/10.1007/s00382-013-1781-1.

Richardson, T. B., and Coauthors, 2018: Drivers of precipitation change: An energetic understanding. *J. Climate*, **31**, 9641–9657, https://doi.org/10.1175/JCLI-D-17-0240.1.

Rodgers, K. B., and Coauthors, 2021: Ubiquity of human-induced changes in climate variability. *Earth Syst. Dyn.*, **12**, 1393–1411, https://doi.org/10.5194/esd-12-1393-2021.

Samset, B. H., and Coauthors, 2018: Weak hydrological sensitivity to temperature change over land, independent of climate forcing. *npj Climate Atmos. Sci.*, **1**, 20173, https://doi.org/10.1038/s41612-017-0005-5.

Schneider, T., P. A. O'Gorman, and X. J. Levine, 2010: Water vapor and the dynamics of climate changes. *Rev. Geophys.*, **48**, RG300, https://doi.org/10.1029/2009RG000302.

Seager, R., N. Naik, and G. A. Vecchi, 2010: Thermodynamic and dynamic mechanisms for large-scale changes in the hydrological cycle in response to global warming. *J. Climate*, **23**, 4651–4668, https://doi.org/10.1175/2010JCLI3655.1.

Sellers, P. J., and Coauthors, 1996: Comparison of radiative and physiological effects of doubled atmospheric CO_2 on climate. *Science*, **271**, 1402–1406, https://doi.org/10.1126/science.271.5254.1402.

Seneviratne, S. I., D. Lüthi, M. Litschi, and C. Schär, 2006: Land–atmosphere coupling and climate change in Europe. *Nature*, **443**, 205–209, https://doi.org/10.1038/nature05095.

——, T. Corti, E. L. Davin, M. Hirschi, E. B. Jaeger, I. Lehner, B. Orlowsky, and A. J. Teuling, 2010: Investigating soil moisture–climate interactions in a changing climate: A review. *Earth. Sci. Rev.*, **99**, 125–161, https://doi.org/10.1016/j.earscirev.2010.02.004.

——, and Coauthors, 2013: Impact of soil moisture-climate feedbacks on CMIP5 projections: First results from the GLACE-CMIP5 experiment. *Geophys. Res. Lett.*, **40**, 5212–5217, https://doi.org/10.1002/grl.50956.

Sherwood, S. C., S. Bony, and J.-L. Dufresne, 2014: Spread in model climate sensitivity traced to atmospheric convective mixing. *Nature*, **505**, 37–42, https://doi.org/10.1038/nature12829.

——, and Coauthors, 2020: An assessment of Earth's climate sensitivity using multiple lines of evidence. *Rev. Geophys.*, **58**, e2019RG000678, https://doi.org/10.1029/2019RG000678.

Shukla, J., and Y. Mintz, 1982: Influence of land-surface evapotranspiration on the Earth's climate. *Science*, **215**, 1498–1501, https://doi.org/10.1126/science.215.4539.1498.

Siler, N., G. H. Roe, K. C. Armour, and N. Feldl, 2019: Revisiting the surface-energy-flux perspective on the sensitivity of global precipitation to climate change. *Climate Dyn.*, **52**, 3983–3995, https://doi.org/10.1007/s00382-018-4359-0.

——, D. B. Bonan, and A. Donohoe, 2023: Diagnosing mechanisms of hydrologic change under global warming in the CESM1 large ensemble. *J. Climate*, **36**, 8243–8257, https://doi.org/10.1175/JCLI-D-23-0086.1.

Skinner, C. B., C. J. Poulsen, R. Chadwick, N. S. Diffenbaugh, and R. P. Fiorella, 2017: The role of plant CO_2 physiological forcing in shaping future daily-scale precipitation. *J. Climate*, **30**, 2319–2340, https://doi.org/10.1175/JCLI-D-16-0603.1.

Stephens, G. L., and T. D. Ellis, 2008: Controls of global-mean precipitation increases in global warming GCM experiments. *J. Climate*, **21**, 6141–6155, https://doi.org/10.1175/2008JCLI2144.1.

——, and Coauthors, 2010: Dreary state of precipitation in global models. *J. Geophys. Res.*, **115**, D24211, https://doi.org/10.1029/2010JD014532.

Swann, A. L. S., F. M. Hoffman, C. D. Koven, and J. T. Randerson, 2016: Plant responses to increasing CO_2 reduce estimates of climate impacts on drought severity. *Proc. Natl. Acad. Sci. USA*, **113**, 10 019–10 024, https://doi.org/10.1073/pnas.1604581113.

Trenberth, K. E., L. Smith, T. Qian, A. Dai, and J. Fasullo, 2007: Estimates of the global water budget and its annual cycle using observational and model data. *J. Hydrometeor.*, **8**, 758–769, https://doi.org/10.1175/JHM600.1.

van der Drift, R. J., and P. A. O'Gorman, 2025: Dependence of convective precipitation extremes on near-surface relative humidity. *J. Climate*, **38**, 6207–6225, https://doi.org/10.1175/JCLI-D-24-0738.1.

Vial, J., J.-L. Dufresne, and S. Bony, 2013: On the interpretation of inter-model spread in CMIP5 climate sensitivity estimates. *Climate Dyn.*, **41**, 3339–3362, https://doi.org/10.1007/s00382-013-1725-9.

Wilks, D. S., 2016: "The stippling shows statistically significant grid points": How research results are routinely overstated and overinterpreted, and what to do about it. *Bull. Amer. Meteor. Soc.*, **97**, 2263–2273, https://doi.org/10.1175/BAMS-D-15-00267.1.

Zarakas, C. M., A. L. S. Swann, M. M. Laguë, K. C. Armour, and J. T. Randerson, 2020: Plant physiology increases the magnitude and spread of the transient climate response to CO_2 in CMIP6 Earth system models. *J. Climate*, **33**, 8561–8578, https://doi.org/10.1175/JCLI-D-20-0078.1.

——, ——, and D. S. Battisti, 2024a: Land-atmosphere feedbacks dampen surface evapotranspiration fluxes in wet regions. ESS Open Archive, https://doi.org/10.22541/essoar.173386151.15960422/v1.

Brought to you by University of Washington Libraries | Unauthenticated | Downloaded 11/20/26 03:51 PM UTC

——, and Coauthors, 2024b: Land processes can substantially impact the mean climate state. *Geophys. Res. Lett.*, **51**, e2024GL108372, https://doi.org/10.1029/2024GL108372.

Zelinka, M. D., T. A. Myers, D. T. McCoy, S. Po-Chedley, P. M. Caldwell, P. Ceppi, S. A. Klein, and K. E. Taylor, 2020: Causes of higher climate sensitivity in CMIP6 models. *Geophys. Res. Lett.*, **47**, e2019GL085782, https://doi.org/10.1029/2019GL085782.

Zhang, X., and Coauthors, 2024: Quantifying global hydrological sensitivity to CO_2 physiological and radiative forcings under large CO_2 increases. *Earth's Future*, **12**, e2023EF004246, https://doi.org/10.1029/2023EF004246.

Zhou, S., and Coauthors, 2021: Soil moisture–atmosphere feedbacks mitigate declining water availability in drylands. *Nat. Climate Change*, **11**, 38–44, https://doi.org/10.1038/s41558-020-00945-z.

Zhou, W., L. R. Leung, and J. Lu, 2023: The role of interactive soil moisture in land drying under anthropogenic warming. *Geophys. Res. Lett.*, **50**, e2023GL105308, https://doi.org/10.1029/2023GL105308.

——, ——, B. E. Harrop, Z. Chen, and C.-C. Chang, 2026: A theoretical index for understanding distinct land relative humidity trends in observations, reanalyses, and models. *Proc. Natl. Acad. Sci. USA*, **123**, e2512645123, https://doi.org/10.1073/pnas.2512645123.

Brought to you by University of Washington Libraries | Unauthenticated | Downloaded 11/20/26 03:51 PM UTC